Microelectronic Engineering 266 (2022) 111888

Contents lists available at ScienceDirect

Microelectronic Engineering

journal homepage: www.elsevier.com/locate/mee

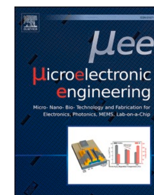

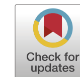

Growth chemistry and electrical performance of ultrathin alumina formed by area selective vapor phase infiltration

M. Snelgrove [a,*], C. McFeely [a], G. Hughes [a], C. Weiland [b], J.C. Woicik [b], K. Shiel [a], P.G. Mani González [c], C. Ornelas [d], Ó. Solís-Canto [d], K. Cherkaoui [e], P.K. Hurley [e], P. Yadav [f], M.A. Morris [f], E. McGlynn [a], R. O'Connor [a]

[a] School of Physical Sciences, Dublin City University, Dublin 9, Ireland
[b] Materials Measurement Science Division, Material Measurement Laboratory, National Institute of Standards and Technology, Gaithersburg, MD 20899, USA
[c] Institute of Engineering and Technology, Department of Physics and Mathematics, Autonomous University of Ciudad Juárez, Cd. Juárez, Chihuahua 32310, Mexico
[d] Centro de Investigacion en Materiales Avanzados, Unidad Chihuahua, Chihuahua 31109, Mexico
[e] Tyndall National Institute, University College Cork, Lee Maltings, Prospect Row, Cork, Ireland
[f] AMBER Research Centre and School of Chemistry, Trinity College Dublin, Dublin, Ireland

ARTICLE INFO

Keywords:
Area selective deposition
Vapor phase infiltration
Polymer
High-k dielectric
Poly(2-vinylpyridine)
Atomic layer deposition

ABSTRACT [1]

The growth chemistry and electrical performance of 5 nm alumina films, fabricated via the area-selective vapor phase infiltration (VPI) of trimethylaluminum into poly(2-vinylpyridine), are compared to a conventional plasma enhanced atomic layer deposition (PEALD) process. The chemical properties are assessed via energy dispersive X-ray spectroscopy and hard X-ray photoelectron spectroscopy measurements, while current – voltage dielectric breakdown and capacitance – voltage analysis is undertaken to provide electrical information of these films for the first time. The success and challenges in dielectric formation via polymer VPI, the compatibility of pyridine in such a role, and the ability of the unique and rapid grafting-to polymer brush method in forming coherent metal oxides is evaluated. It was found that VPI made alumina fabricated at temperatures between 200 and 250 °C had a consistent breakdown electrical field, with the best performing devices possessing a κ value of 5.9. The results indicate that the VPI approach allows for the creation of alumina films that display dielectric properties of a comparable quality to conventional PEALD grown films.

1. Introduction

Top-down patterning approaches utilising photolithography have been essential in the continued miniaturization and development of semiconductor components. As devices scale below the 7 nm node, the complexity and cost in current patterning methodologies has led to the desire to develop bottom-up processes such as area selective deposition (ASD) that can replace or complement existing photolithography techniques. [1–5] Such development would combat issues such as production cost while ensuring the continued fabrication of miniaturised devices. [6–8]

Through the use of chemical interactions across a surface, ASD allows for the deposition of a material on certain regions of a surface while simultaneously denying growth in other regions, negating the need for masking steps found in conventional photolithography. [9] One pathway to achieving ASD is through polymer vapor phase infiltration (VPI). The technique involves exposing reactive polymer films to metal-containing precursors commonly used in atomic layer deposition (ALD) processes, with the objective of forming a metal oxide through a two-step process: (1) metal precursor sorption, transport, and entrapment in a polymer film, and (2) polymer removal and metal oxidation through an oxygen rich process. [10] By combining with non-reactive polymers that do not interact with the metal precursor, the process can be implemented into ASD applications through block copolymers (BCP) and covalently grafted polymer brush architecture. [11–13]

While much work has focused on the synthesis and metal-infiltration into BCP/ASD suitable polymers, the electrical performance of the fabricated metal oxides formed via polymer VPI is of critical importance

* Corresponding author.
E-mail address: matthew.snelgrove2@mail.dcu.ie (M. Snelgrove).

[1] Commercial equipment is identified in this report in order to specify the experimental procedure adequately and does not imply recommendation or endorsement by the National Institute of Standards and Technology, nor is it intended to imply that the equipment identified is necessarily the best available for the purpose.

https://doi.org/10.1016/j.mee.2022.111888
Received 12 August 2022; Received in revised form 8 September 2022; Accepted 23 September 2022
Available online 28 September 2022
0167-9317/© 2022 The Authors. Published by Elsevier B.V. This is an open access article under the CC BY license (http://creativecommons.org/licenses/by/4.0/).

if these processes are to be incorporated into semiconductor industry fabrication processes. Studies of metal oxides produced from metal infiltration into polymers for ASD purposes include the comparable resistivity of In_2O_3 grown via Poly(methyl methacrylate) (PMMA) VPI and ALD as reported by Waldman et al., [14] and the successful testing of semiconducting ZnO nanowires obtained via VPI of diethylzinc into patterned SU-8 polymer templates by Nam et al. [15]

Our previous work demonstrated the successful integration of poly (2-vinylpyridine) (P2VP) into a VPI based process for the area selective growth of ultrathin (5 nm) alumina, using trimethylaluminum (TMA) as the only precursor (a co-reactant was not required). [16] P2VP is a reactive polymer in ASD and BCP architecture, due to the nitrogen lone pair in the pyridine ring facilitating metal precursor interaction. P2VP can also facilitate the production of metal structures on the nanometre dimensional scale when incorporated into BCP systems, [17–20] making P2VP a desirable polymer for future ASD applications. However, knowledge concerning the electrical performance of the metal oxide post polymer removal has not been undertaken. This work provides new insight into alumina created via P2VP VPI, assessing the breakdown electrical field, dielectric constant and chemical properties of the film for comparison to a more standard ALD processes.

2. Materials and methods

P2VP-OH (6 kg/mol) brush films, covalently bonded to Si with a native oxide, were prepared using a rapid spin coating process. [21] This involved dissolving hydroxy terminated P2VP (6 kg/mol) (PDI: 1.04) in tetrahydrofuran (THF) to form a 0.2 wt% solution. The solution was spin coated onto p-type Si (piranha treated for OH termination) for 30 s at 3000 rpm. The samples were then annealed for 60 s at 230 °C, before being ultra-sonicated in two baths of THF to remove any physisorbed, ungrafted polymer. Post processing ellipsometry measurements (Woollam XLS-100) confirmed the expected polymer brush thickness of ≈5 nm. [21]

The TMA VPI optimised process involved exposing the P2VP brush to cycles of TMA in an ALD vacuum chamber (Oxford Instruments FlexAl, base pressure: 5×10^{-5} Pa), which was coupled in-vacuum by a fast-transfer robotic handler to a Scienta Omicron X-ray photoemission Spectroscopy (XPS) chamber (monochromatic Al Kα X-ray source, base pressure 6.5×10^{-7} Pa) equipped with a 128 channel Argus CU detector. Transfer time between chambers is 1 min. Prior to entering the ALD chamber for TMA infiltration, the P2VP brush was cleaved to 2 cm^2 in size and exposed to compressed N_2 to remove dust particles. Once in the chamber, the samples were heated for 20 min at the desired substrate temperature (100–250 °C), with the chamber under flow of 200 SCCM Ar gas to ensure good thermal conductivity. The pressure of the chamber at this stage was kept at 26.7 Pa (200 mTorr). The cyclic VPI process could then begin, with one cycle consisting of (1) a 60 ms TMA dose, (2) a 2 min hold step where the chamber was kept in static vacuum and (3) a 20 s TMA purge where pumping resumed and 200 SCCM of Ar was admitted into the chamber. The cycle was repeated until XPS revealed that saturation (no further intake of Al into the polymer) occurred. Polymer removal and Al oxidation was then achieved by a 15 min, 300 W O_2 plasma located in the ALD chamber. The flow of O_2 was 100 SCCM, and the pressure during the plasma process was 5.3 Pa.

The VPI films were fabricated at different temperatures in the range of 100 °C – 250 °C, predetermined to ensure the polymer was well below its degradation temperature (320 °C). [22] The VPI temperatures were also kept at or above the bulk glass transition temperature (T_g) of P2VP (≈100 °C), [23] which consequently minimised the effects of precursor condensation. These 'VPI grown' alumina films were compared to a 200 °C plasma enhanced atomic layer deposition (PEALD) process, involving a 20 ms TMA dose (pressure capped at 11 Pa) and a 300 W O_2 plasma step set at 2 Pa for 2 s on the same p-type silicon. Following all processing steps, both VPI and ALD samples were heated to 400 °C and exposed to a 20 min, 50 sccm flow of Ar to lower the fixed oxide charge. [24] This was immediately followed by a H_2 exposure under the same parameters to reduce interfacial state density (D_{it}) and charge trapping. [25]

To prepare the alumina for electrical characterization, Cu was deposited on the films via thermal evaporation (Edwards E306A) through a Si mask with laser cut square openings. Optical microscopy revealed that this process yielded square contacts of $(8.4 \pm 0.6) \times 10^{-3}$ mm^2.

Sample preparation for transmission electron microscopy (TEM) and energy dispersive X-ray spectroscopy (EDX) was performed by locating a clean defect free area on the sample of interest. A JEM-9320 focused ion beam (FIB) model from Jeol was used to prepare the lamella for TEM characterization. Prior to the thinning, the samples were coated with a gold layer to achieve a good electrical contact using a Dektak II coating system and a FIB-deposited coating layer of carbon to prevent milling and to protect the local interest area. A 30 kV Ga ion beam was used to mill and polish the cross section.

3. Results and discussion

Prior to sample removal from vacuum, the Si/SiO_2/Alumina interface was monitored in-situ by XPS via acquisition of Si 2*p* core level spectra, shown in fig. S1 of the supporting information (SI). The intensities of the Si^0 and Si^{4+} in the Si 2*p* XPS spectra were used in accordance with literature for an estimation of the SiO_2 interlayer thickness. [26] This thickness was calculated as 0.6 nm and 0.7 nm for the PEALD and all VPI films, respectively, for the films post processing (alumina on silicon). All analysis will now be focused on the alumina samples post all processing steps.

Cross-sectional energy dispersive X-ray spectroscopy (EDX) was then performed ex-situ on the 100 °C and 250 °C VPI films and compared to a 35-cycle PEALD film. The resulting images are shown in Fig. 1 (a-c). Combined with cross-sectional TEM, Ellipsometry and XPS, all alumina films are in the range of 5.0 to 5.5 nm in thickness.

Using thicknesses extracted from XPS/TEM/EDX, ellipsometry measurements used a Cauchy model for the calculation of the refractive index (n). [27] The calculated value of n at a wavelength of 650 nm for the PEALD film was determined as 1.48 ± 0.01, while the 100 °C and 250 °C VPI films had similar values of 1.28 ± 0.01 and 1.29 ± 0.01 respectively. The change in refractive index suggests that the alumina films made via the polymer VPI method are less dense than conventional ALD films, correlating with the in-situ XPS measurements further (fig. S2). Such behaviour has been previously witnessed by Cianci et al. during the VPI of TMA into PMMA films. [28]

Hard X-ray photoelectron spectroscopy (HAXPES) core level spectra in Fig. 1 (d-e) compares the PEALD film to the 250 °C and 100 °C VPI processed films. The measurements were obtained at the National Institute of Standards and Technology beamline 7-ID-2, located at the National Synchrotron Light Source II (NSLS-II), Brookhaven, New York. A photon energy of 2.4 keV was used, with samples placed 5° from normal emission. The Si 2*p* was fitted in accordance to the literature, with the binding energy positions and peak widths fixed (with the exception of the Si^{4+} position). [29,30] All spectra have been charge referenced so that the Si $2p_{3/2}$ bulk peak (Si^0), shown in Fig. 1 (d), for each dataset occurs at 99.4 eV binding energy. [31] Despite all processes using the same Si substrate, the intensity of the Si^{4+} peak is higher for the VPI films, with more intense Si^{3+} and Si^{1+} states witnessed also. These results cross compare well to the in-situ Si 2*p* spectra taken immediately after processing (Fig. S1). The plasma treatment during the polymer removal/metal oxidation process is attributed to the main cause of Si^{4+} growth, while increased Si dioxide – alumina interaction explains the increased sub oxide presence for the VPI films. [32,33] These effects demonstrate that the VPI process has more impact on the SiO_2/Alumina interface than the PEALD film, which has relevance to the following CV analysis.

No chemical difference in the alumina can be extracted between the

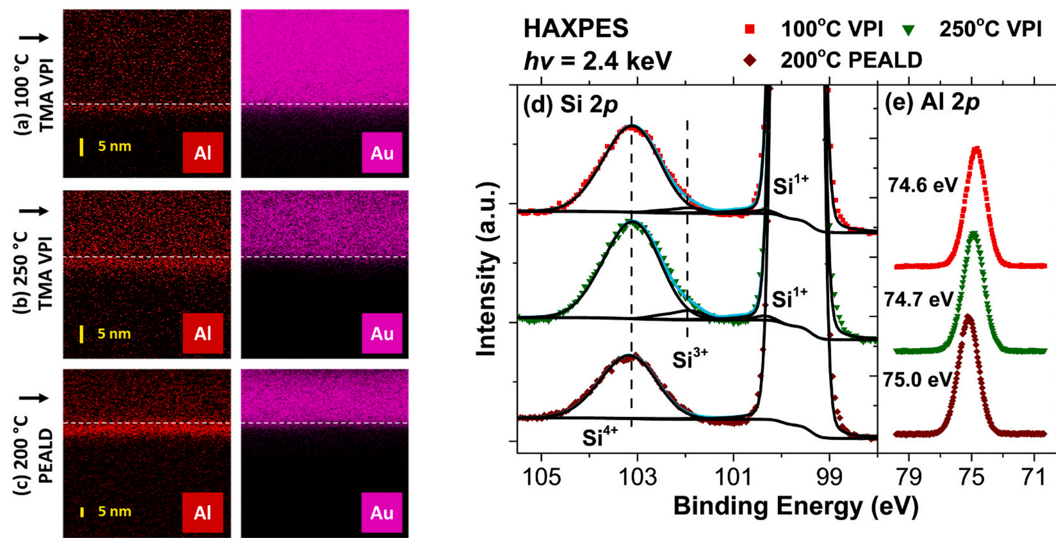

Fig. 1. (a-c) EDX cross sectional images of (a) 100 °C VPI, (b) 250 °C VPI and (c) 200 °C PEALD. Elemental maps of Al and the Au capping layer are shown. (d-e) HAXPES spectra of (d) Si 2*p* and (e) Al 2p. Peak maxima positions for the Al 2*p* are labelled.

different VPI temperatures via photoemission. As in the O 1 *s* spectra (fig. S3), a slight shift (0.2–0.3 eV) to higher binding energy is observed in the peak maxima position for the Al 2*p* spectra in Fig. 1 (e) for the PEALD film. The range of binding energy positions for the Al_2O_3 in Al 2*p* spectra is broad, with reported positions overlapping with the hydroxides $Al(OH)_3$ and AlO(OH) according to the NIST database. [34] Due to the presence of OH in the FTIR spectra (fig. S4), it is reasonable to conclude the presence of significant hydroxyl groups in all films. Additionally, OH groups in the alumina film are reported to cause a shift to higher binding energy both in aluminium and oxygen core level spectra. [32–36] It can therefore be concluded that the PEALD film contains a higher amount of hydroxyl groups, arising from the growth process within the ALD chamber. Previous work in PEALD of alumina using TMA has reported increased concentrations of oxygen and hydrogen in the film, particularly at temperatures below 200 °C. [37,38] This effect is not attributed to differences in adsorbed water on the surface post atmosphere exposure, because the shift was also observed before samples left vacuum.

Current – voltage (IV) plots were obtained to compare the breakdown electric field (E_b) of the VPI method to PEALD. Each process was analysed twice – with one Weibull distribution corresponding to testing across multiple sites on a single sample. Sample IV plots displaying the breakdown voltage (V_b) are shown in Fig. S5 of the SI. The resulting Weibull distributions of E_b are shown in Fig. 2 (a). Only datasets with a clear breakdown (as demonstrated in Fig. S5) contributed to the distribution. The Weibull slope (β) and the 63% breakdown field value (E_α) are displayed in the plot legend.

It has been reported that the breakdown field of ALD grown Al_2O_3 is typically in the range of 5 MV/cm to 10 MV/cm. [39,40] While a high breakdown field is a desired result, indicating electrically insulating Al_2O_3 has been obtained, caution must be applied as the capacitors are effectively a bi-layer oxide stack. The presence of an interlayer of SiO_2 is expected to have an impact on the breakdown field even at thicknesses below 1 nm, [41] with increasing breakdown fields as the SiO_2 interlayer thickness increases. Our results show the breakdown field of the 250 °C and 200 °C VPI processes fall within the expected range (6.2–7.5 MV/cm), with a β value between 0.94 and 2.22. The 100 °C VPI sample breakdown exceeds this (8.9–12.3 MV/cm), but possesses the lowest β value (0.54–0.60), indicating this VPI process temperature is the most inconsistent electrically. The PEALD sample breakdown field was determined as the highest (11.8–13.9 MV/cm), with a β value determined between 0.60 and 0.74.

Capacitance – voltage (CV) profiles taken at 120 kHz are shown in Fig. 2 (b), where each sample was scanned from inversion to

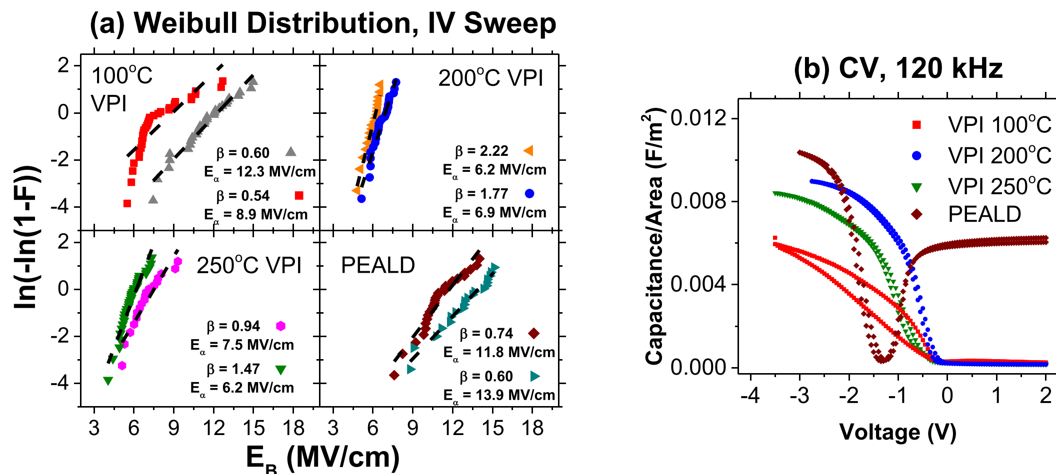

Fig. 2. (a) Weibull distribution of E_B. E_α and β values shown. A single distribution represents testing across multiple sites on a single sample, with 2 samples per process analysed. (b) Sample CV sweep. Multiple sweeps were performed at different sites for each sample.

accumulation (trace) and back (retrace). The CV profile for the 100 °C VPI film was impacted by a significant amount of hysteresis. This hysteresis is linked to trapped charge in the film, which is causing this film to have a lower accumulation capacitance (C_{acc}). This result may also explain the high E_B and inconsistent behaviour observed of the 100 °C VPI film for the IV analysis. A notable feature from Fig. 2 (b) is that the level of CV hysteresis for the 200 °C and 250 °C VPI samples is lower than the PEALD sample, indicating a lower density of defects in the 200 °C and 250 °C VPI samples which have capture and emission time constants longer than the time associated with the CV sweep.

To determine the dielectric constant of the alumina films, ($\kappa_{alumina}$), $C_{alumina}$ was determined from $1/C_{acc} = 1/C_{SiO2} + 1/C_{alumina}$. The accumulation capacitance was measured across multiple sites for each sample. C_{SiO2} was calculated theoretically, with the assumption that the κ value for the SiO_2 layer for both films was 3.9. [42] The calculated κ value for the PEALD film at 120 kHz was determined as 5.0 ± 1.1, which was surpassed by the VPI 250 °C (5.4 ± 0.3) and VPI 200 °C (5.9 ± 0.9) films (the VPI 100 °C was lower at 3.9 ± 0.6, but disregarded due to the large amount of trapped charge). While smaller contacts are desired for a potentially more accurate assessment of the true κ value, the ability of the VPI approach to compete with the PEALD film is observed.

All VPI films contained an extended transition from inversion to accumulation, when compared to the PEALD film. This suggests a higher concentration of D_{it} are present via the VPI approach. [43–45] This correlates with the observations seen in the HAXPES Si 2*p* analysis in Fig. 1 (d) – the impact that the VPI process has at the Si/SiO_2/alumina interface, at any temperature, causes a degradation in the performance of the VPI films as capacitors.

It is also noted that a significant inversion capacitance is observed on the PEALD film, despite the high frequency (120 kHz) range used. This is not expected for typical minority carrier lifetimes in silicon, [46] and has been previously attributed to 'peripheral inversion' where charge exists in the oxide (both at the surface and within the layer) in the region outside the area under the gate electrode. [47] This effect has previously been witnessed for Al_2O_3 on Si processed via ALD, at annealing temperatures of 500 °C. [48] Combined with the negative flatband shift seen only in the PEALD film, there appears to be an abundance of positive charge. This is despite the use of O_2 plasma for both processes, and the increased hydroxyl presence observed via HAXPES in the PEALD film.

4. Conclusions

Alumina films fabricated via an area selective process implementing the VPI of TMA into P2VP films have been characterised chemically and electrically, with several key points observed for the further improvement of the VPI film performance. The process has been shown to produce alumina films that have electrical properties that closely resemble PEALD films grown in a similar temperature regime. The VPI films processed in the temperature range of 200–250 °C had a highly consistent breakdown field during IV sweeps, surpassing the PEALD reference in reliability. While the PEALD film can be associated with a higher overall breakdown voltage, the 200–250 °C VPI films matched it when calculating the κ value from C_{acc}. It can also be concluded that lower temperature VPI films result in undesirable effects such as a large E_B distribution, low C_{acc} and a high concentration of trapped charge. Finally, it was found that the VPI films can be further optimised if the densification of the VPI made alumina, and the reduction of D_{it} present in the film is enacted. Investigating parameters such as polymer molecular weight may address the former, while the reduction of D_{it} may be overcome through optimisation of the polymer removal/metal oxidation step of the VPI process.

CRediT authorship contribution statement

M. Snelgrove: Formal analysis, Investigation, Methodology, Writing – original draft. **C. McFeely:** Investigation, Methodology, Writing – review & editing. **G. Hughes:** Investigation, Supervision, Writing – review & editing. **C. Weiland:** Investigation, Methodology, Writing – review & editing. **J.C. Woicik:** Investigation, Methodology, Writing – review & editing. **K. Shiel:** Investigation, Methodology. **P.G. Mani González:** Investigation, Writing – review & editing. **C. Ornelas:** Investigation. **Ó. Solís-Canto:** Investigation. **K. Cherkaoui:** Formal analysis, Writing – review & editing. **P.K. Hurley:** Formal analysis, Writing – review & editing. **P. Yadav:** Investigation, Methodology. **M.A. Morris:** Conceptualization, Writing – review & editing. **E. McGlynn:** Conceptualization, Supervision, Writing – review & editing. **R. O'Connor:** Formal analysis, Conceptualization, Supervision, Writing – review & editing.

Declaration of Competing Interest

The authors declare that they have no known competing financial interests or personal relationships that could have appeared to influence the work reported in this paper.

Data availability

Data will be made available on request.

Acknowledgements

This publication has emanated from research conducted with the financial support of Science Foundation Ireland (SFI) under Grant No. 12/RC/2278 and 16/SP/3809. The authors would like to thank the NSLS-II for the use of their facilities in making experimental measurements as well as the support given by the beamline scientists (NSLS-II proposal number 307840) and the National Institute of Standards and Technology (NIST). This research used NIST beamline 7-ID-2 of NSLS-II, a U.S. Department of Energy (DOE) Office of Science User Facility operated for the DOE Office of Science by Brookhaven National Laboratory under Contract No. DE-SC0012704.

Appendix A. Supplementary data

Supplementary data to this article can be found online at https://doi.org/10.1016/j.mee.2022.111888.

References

[1] R. Chen, Y.C. Li, J.M. Cai, K. Cao, H.B.R. Lee, Atomic level deposition to extend Moore's law and beyond, Int. J. Extrem. Manuf. 2 (2020), 022002, https://doi.org/10.1088/2631-7990/ab83e0.
[2] A.J.M. Mackus, M.J.M. Merkx, W.M.M. Kessels, From the bottom-up: toward area-selective atomic layer deposition with high selectivity †, Chem. Mater. 31 (2019) 2–12, https://doi.org/10.1021/acs.chemmater.8b03454.
[3] R.K. Ratnesh, A. Goel, G. Kaushik, H. Garg, M. Chandan, B. Prasad Singh, Advancement and challenges in MOSFET scaling, Mater. Sci. Semicond. Process. 134 (2021), 106002, https://doi.org/10.1016/j.mssp.2021.106002.
[4] R.M.M. Hasan, X. Luo, Promising lithography techniques for next-generation logic devices, Nanomanuf. Metrol. 1 (2018) 67–81, https://doi.org/10.1007/s41871-018-0016-9.
[5] B.J. Lin, Making lithography work for the 7-nm node and beyond in overlay accuracy, resolution, defect, and cost, Microelectron. Eng. 143 (2015) 91–101, https://doi.org/10.1016/j.mee.2015.04.033.
[6] M.A. Morris, Directed self-assembly of block copolymers for nanocircuitry fabrication, Microelectron. Eng. 132 (2015) 207–217, https://doi.org/10.1016/j.mee.2014.08.009.
[7] A. Biswas, I.S. Bayer, A.S. Biris, T. Wang, E. Dervishi, F. Faupel, Advances in top-down and bottom-up surface nanofabrication: techniques, applications & future prospects, Adv. Colloid Interf. Sci. 170 (2012) 2–27, https://doi.org/10.1016/j.cis.2011.11.001.
[8] R. Clark, K. Tapily, K.H. Yu, T. Hakamata, S. Consiglio, D. O'Meara, C. Wajda, J. Smith, G. Leusink, Perspective: new process technologies required for future devices and scaling, APL Mater. 6 (2018) 58203, https://doi.org/10.1063/1.5026805.
[9] G.N. Parsons, R.D. Clark, Area-selective deposition: fundamentals, applications, and future outlook, Chem. Mater. 32 (2020) 4920–4953, https://doi.org/10.1021/ACS.CHEMMATER.0C00722/ASSET/IMAGES/LARGE/CM0C00722_0006.JPEG.

[10] C.Z. Leng, M.D. Losego, Vapor phase infiltration (VPI) for transforming polymers into organic-inorganic hybrid materials: a critical review of current progress and future challenges, Mater. Horizon 4 (2017) 747–771, https://doi.org/10.1039/c7mh00196g.

[11] E. Cara, I. Murataj, G. Milano, N. De Leo, L. Boarino, F.F. Lupi, Recent advances in sequential infiltration synthesis (Sis) of block copolymers (bcps), Nanomaterials. 11 (2021) 994, https://doi.org/10.3390/nano11040994.

[12] C. Cummins, M.T. Shaw, M.A. Morris, Area selective polymer brush deposition, Macromol. Rapid Commun. 38 (2017) 1700252, https://doi.org/10.1002/marc.201700252.

[13] R.Z. Waldman, D.J. Mandia, A. Yanguas-Gil, A.B.F. Martinson, J.W. Elam, S. B. Darling, The chemical physics of sequential infiltration synthesis - a thermodynamic and kinetic perspective, J. Chem. Phys. 151 (2019), 190901, https://doi.org/10.1063/1.5128108.

[14] R.Z. Waldman, N. Jeon, D.J. Mandia, O. Heinonen, S.B. Darling, A.B.F. Martinson, Sequential infiltration synthesis of electronic materials: group 13 oxides via metal alkyl precursors, Chem. Mater. 31 (2019) 5274–5285, https://doi.org/10.1021/acs.chemmater.9b01714.

[15] C.Y. Nam, A. Stein, K. Kisslinger, C.T. Black, Electrical and structural properties of ZnO synthesized via infiltration of lithographically defined polymer templates, Appl. Phys. Lett. 107 (2015), https://doi.org/10.1063/1.4935793.

[16] M. Snelgrove, C. McFeely, K. Shiel, G. Hughes, P. Yadav, C. Weiland, J.C. Woicik, P.G. Mani-Gonzalez, R. Lundy, M.A. Morris, E. McGlynn, R. O'Connor, Analysing trimethylaluminum infiltration into polymer brushes using a scalable area selective vapor phase process, Mater. Adv. 2 (2021) 769–781, https://doi.org/10.1039/d0ma00928h.

[17] C. Sinturel, F.S. Bates, M.A. Hillmyer, High χ-low N block polymers: how far can we go? ACS Macro Lett. 4 (2015) 1044–1050, https://doi.org/10.1021/acsmacrolett.5b00472.

[18] Y. Kim, W. Lee, S. Jo, H. Ahn, K. Kim, J.U. Kim, D.Y. Ryu, Lamellar orientation and transition behavior of PS- b-P2VP copolymers supported on physically adsorbed layers, Macromolecules. 53 (2020) 6213–6219, https://doi.org/10.1021/acs.macromol.0c00794.

[19] J.G. Kennemur, Poly(vinylpyridine) segments in block copolymers: synthesis, self-assembly, and versatility, Macromolecules. 52 (2019) 1354–1370, https://doi.org/10.1021/acs.macromol.8b01661.

[20] S. Xiong, L. Wan, Y. Ishida, Y.A. Chapuis, G.S.W. Craig, R. Ruiz, P.F. Nealey, Directed self-assembly of triblock copolymer on chemical patterns for Sub-10-nm nanofabrication via solvent annealing, ACS Nano 10 (2016) 7855–7865, https://doi.org/10.1021/acsnano.6b03667.

[21] R. Lundy, P. Yadav, N. Prochukhan, E.C. Giraud, T.F. O'Mahony, A. Selkirk, E. Mullen, J. Conway, M. Turner, S. Daniels, P.G. Mani-Gonzalez, M. Snelgrove, J. Bogan, C. McFeely, R. O'Connor, E. McGlynn, G. Hughes, C. Cummins, M. A. Morris, Precise definition of a "monolayer point" in polymer brush films for fabricating highly coherent TiO2 thin films by vapor-phase infiltration, Langmuir. 36 (2020) 12394–12402, https://doi.org/10.1021/acs.langmuir.0c02512.

[22] R. Lundy, P. Yadav, A. Selkirk, E. Mullen, T. Ghoshal, C. Cummins, M.A. Morris, Optimizing polymer brush coverage to develop highly coherent Sub-5 nm oxide films by ion inclusion, Chem. Mater. 31 (2019) 9338–9345, https://doi.org/10.1021/acs.chemmater.9b02856.

[23] N. Jiang, M. Sen, M.K. Endoh, T. Koga, E. Langhammer, P. Bjöörn, M. Tsige, Thermal properties and segmental dynamics of polymer melt chains adsorbed on solid surfaces, Langmuir. 34 (2018) 4199–4209, https://doi.org/10.1021/acs.langmuir.8b00122.

[24] B.E. Deal, M. Sklar, A.S. Grove, E.H. Snow, Characteristics of the surface-state charge (Qss) of thermally oxidized silicon, J. Electrochem. Soc. 114 (1967) 266, https://doi.org/10.1149/1.2426565.

[25] W.J. Cho, R. Kosugi, K. Fukuda, K. Arai, S. Suzuki, Improvement of charge trapping by hydrogen post-oxidation annealing in gate oxide of 4H-SiC metal-oxide-semiconductor capacitors, Appl. Phys. Lett. 77 (2000) 1215–1217, https://doi.org/10.1063/1.1289806.

[26] D.S. Jensen, S.S. Kanyal, N. Madaan, M.A. Vail, A.E. Dadson, M.H. Engelhard, M. R. Linford, Silicon (100)/SiO 2 by XPS, Surf. Sci. Spectra 20 (2013) 36–42, https://doi.org/10.1116/11.20121101.

[27] H.G. Tompkins, E.A. Irene, Handbook of Ellipsometry, William Andrew, New York, 2005 file:///Users/alex.neumann/Documents/Mendeley Desktop/Edited by Edited by/World/[Darren_Swanson]_Creating_Adaptive_Policies_A_Gui(BookSee.org).pdf.

[28] E. Cianci, D. Nazzari, G. Seguini, M. Perego, Trimethylaluminum diffusion in PMMA thin films during sequential infiltration synthesis: in situ dynamic spectroscopic ellipsometric investigation, Adv. Mater. Interfaces 5 (2018) 1801016, https://doi.org/10.1002/admi.201801016.

[29] J.C. Woicik, P. Pianetta, T. Kendelewicz, Si(111) 2 X 1 surface core-level shifts investigated by use of Ge overlayer, Phys. Rev. B 40 (1989) 12463–12467, https://doi.org/10.1103/physrevb.40.12463.

[30] F.J. Himpsel, F.R. McFeely, A. Taleb-Ibrahimi, J.A. Yarmoff, G. Hollinger, Microscopic structure of the SiO2/Si interface, Phys. Rev. B 38 (1988) 6084–6096, https://doi.org/10.1103/PhysRevB.38.6084.

[31] A. Herrera-Gomez, Y. Sun, F.-S. Aguirre-Tostado, C. Hwang, P.-G. Mani-Gonzalez, E. Flint, F. Espinosa-Magaña, R.M. Wallace, Structure of ultra-thin diamond-like carbon films grown with filtered cathodic arc on Si(001), Anal. Sci. 26 (2010) 267–272, https://doi.org/10.2116/analsci.26.267.

[32] G.P. Gakis, C. Vahlas, H. Vergnes, S. Dourdain, Y. Tison, H. Martinez, J. Bour, D. Ruch, A.G. Boudouvis, B. Caussat, E. Scheid, Investigation of the initial deposition steps and the interfacial layer of atomic layer deposited (ALD) Al2O3 on Si, Appl. Surf. Sci. 492 (2019) 245–254, https://doi.org/10.1016/j.apsusc.2019.06.215.

[33] O. Renault, L.G. Gosset, D. Rouchon, A. Ermolieff, Angle-resolved x-ray photoelectron spectroscopy of ultrathin Al2O3 films grown by atomic layer deposition, J. Vac. Sci. Technol. A 20 (2002) 1867, https://doi.org/10.1116/1.1507330.

[34] National Institute of Standards and Technology, NIST X-ray Photoelectron Spectroscopy Database. http://srdata.nist.gov/xps/, 2012.

[35] I. Iatsunskyi, M. Kempiński, M. Jancelewicz, K. Załęski, S. Jurga, V. Smyntyna, Structural and XPS characterization of ALD Al2O3 coated porous silicon, Vacuum. 113 (2015) 52–58, https://doi.org/10.1016/j.vacuum.2014.12.015.

[36] C. Fan, C. Chen, J. Wang, X. Fu, Z. Ren, G. Qian, Z. Wang, Black hydroxylated titanium dioxide prepared via ultrasonication with enhanced photocatalytic activity, Sci. Rep. 5 (2015) 11712, https://doi.org/10.1038/srep11712.

[37] J.L. van Hemmen, S.B.S. Heil, J.H. Klootwijk, F. Roozeboom, C.J. Hodson, M.C. M. van de Sanden, W.M.M. Kessels, Plasma and thermal ALD of Al2O3 in a commercial 200 mm ALD reactor, J. Electrochem. Soc. 154 (2007) G165, https://doi.org/10.1149/1.2737629.

[38] E. Langereis, J. Keijmel, M.C.M. Van De Sanden, W.M.M. Kessels, Surface chemistry of plasma-assisted atomic layer deposition of Al2O3 studied by infrared spectroscopy, Appl. Phys. Lett. 92 (2008), 231904, https://doi.org/10.1063/1.2940598.

[39] H.C. Lin, P.D. Ye, G.D. Wilk, Leakage current and breakdown electric-field studies on ultrathin atomic-layer-deposited Al2O3 on GaAs, Appl. Phys. Lett. 87 (2005), 182904, https://doi.org/10.1063/1.2120904.

[40] J. Yota, H. Shen, R. Ramanathan, Characterization of atomic layer deposition HfO2, Al2O3, and plasma-enhanced chemical vapor deposition Si3N4 as metal–insulator–metal capacitor dielectric for GaAs HBT technology, J. Vac. Sci. Technol. A 31 (2013) 01A134, https://doi.org/10.1116/1.4769207.

[41] B.H. Lee, C. Kang, R. Choi, H.D. Lee, G. Bersuker, Stress field analysis to understand the breakdown characteristics of stacked high- k dielectrics, Appl. Phys. Lett. 94 (2009), 162904, https://doi.org/10.1063/1.3122924.

[42] J. Robertson, High dielectric constant oxides, Eur. Phys. J. Appl. Phys. 28 (2004) 265–291, https://doi.org/10.1051/epjap:2004206.

[43] C. Byrne, B. Brennan, R. Lundy, J. Bogan, A. Brady, Y.Y. Gomeniuk, S. Monaghan, P.K. Hurley, G. Hughes, Physical, chemical and electrical characterisation of the diffusion of copper in silicon dioxide and prevention via a CuAl alloy barrier layer system, Mater. Sci. Semicond. Process. 63 (2017) 227–236, https://doi.org/10.1016/j.mssp.2017.02.024.

[44] D.K. Schroder, Semiconductor and Device Characterization, 3rd ed., John Wiley & Sons, Hoboken, 2006.

[45] D. Misra, High k dielectrics on high-mobility substrates: the interface!, Electrochem. Soc. Interface 20 (2011) 47–51, https://doi.org/10.1149/2.F05114if.

[46] P. Batude, X. Garros, L. Clavelier, C. Le Royer, J.M. Hartmann, V. Loup, P. Besson, L. Vandroux, Y. Campidelli, S. Deleonibus, F. Boulanger, Insights on fundamental mechanisms impacting Ge metal oxide semiconductor capacitors with high-k/metal gate stacks, J. Appl. Phys. 102 (2007), 034514, https://doi.org/10.1063/1.2767381.

[47] E. O'Connor, K. Cherkaoui, S. Monaghan, D. O'Connell, I. Povey, P. Casey, S. B. Newcomb, Y.Y. Gomeniuk, G. Provenzano, F. Crupi, G. Hughes, P.K. Hurley, Observation of peripheral charge induced low frequency capacitance-voltage behaviour in metal-oxide-semiconductor capacitors on Si and GaAs substrates, J. Appl. Phys. 111 (2012), 124104, https://doi.org/10.1063/1.4729331.

[48] J.P. Lehtiö, Z.J. Rad, S. Granroth, M. Yasir, M. Punkkinen, R. Punkkinen, H. P. Hedman, J.P. Rueff, I.T.S. Rauha, H. Savin, P. Laukkanen, K. Kokko, Observation of Si 2p core-level shift in Si/high-κ dielectric interfaces containing a negative charge, Adv. Electron. Mater. 7 (2021) 2100034, https://doi.org/10.1002/aelm.202100034.